Journal of
Applied
Crystallography

ISSN 0021-8898

Received 30 January 2001
Accepted 5 June 2001

Application of the reverse Monte Carlo method to crystalline materials

Matthew G. Tucker,[a] Martin T. Dove[a]* and David A. Keen[b]

[a]Mineral Physics Group, Department of Earth Sciences, University of Cambridge, Downing Street, Cambridge CB2 3EQ, England, and [b]ISIS Facility, Rutherford Appleton Laboratory, Chilton, Didcot, Oxfordshire OX11 0QX, England. Correspondence e-mail: martin@esc.cam.ac.uk

An implementation of the reverse Monte Carlo (RMC) method for the study of crystalline materials from polycrystalline neutron total scattering data is presented. The new feature is that explicit account is taken of the intensities of Bragg peaks, which are extracted from the data using the Pawley method. The use of Bragg peaks ensures that the RMC models reproduce both the long-range and the short-range order reflected in the experimental data. The relative effects of different contributions to the data sets in the RMC method are assessed and successful applications are illustrated using the quartz and cristobalite polymorphs of silica as examples.

1. Introduction

1.1. The reverse Monte Carlo method and its application to crystalline materials

The reverse Monte Carlo (RMC) method was first developed by McGreevy & Pusztai (1988) as an approach for building atomic models based on diffraction data rather than interatomic potentials. It was primarily designed for the study of liquids and amorphous materials because of the lack of other routes to obtain structural information in such cases, but the method is, at least in principle, capable of providing a powerful analysis tool for modelling crystalline systems.

The RMC method, at its most basic level, is a simulation approach in which the positions of atoms in a configuration with periodic boundary conditions can be moved until the calculated diffraction pattern (or its Fourier transform) matches the experimental data. The basic equation of diffraction is the scattering law:

$$S(\mathbf{Q}) = \sum_{i,j} b_i b_j \langle \exp[i\,\mathbf{Q}\cdot(\mathbf{r}_i - \mathbf{r}_j)]\rangle. \qquad (1)$$

This contains information about the relative positions of pairs of atoms, as given by $\mathbf{r}_i - \mathbf{r}_j$. This information is exactly what is needed in the study of liquids and amorphous materials, because absolute positions have no meaning. However, the study of the structure of crystals has been dominated by the use of Bragg scattering. Technically, the $S(\mathbf{Q})$ function defined above is an integral over all energies. On the other hand, the Bragg scattering function, which is given as

$$S_{\rm Bragg}(\mathbf{Q}) = \left| \sum_j b_j \langle \exp(i\,\mathbf{Q}\cdot\mathbf{r}_j)\rangle \right|^2, \qquad (2)$$

is equivalent to the elastic (zero energy transfer) component of $S(\mathbf{Q})$ at Bragg hkl positions. $S_{\rm Bragg}(\mathbf{Q})$ contains information about the distribution of atomic positions, but nothing about the instantaneous positions between atoms. For harmonic (or nearly harmonic) crystals, this is not a problem, because the distribution function for the instantaneous distance between any pair of atoms is simply given by the integral over the respective single-particle distribution functions. However, for highly anharmonic or disordered crystals, the distribution function for interatomic separations cannot be obtained directly from Bragg diffraction data. An example is given by our recent work on quartz (Tucker *et al.*, 2000; Tucker, Keen & Dove, 2001). The average positions of the Si and O atoms can be refined by fitting to the Bragg peaks; the distances between these average positions, here labelled $\langle{\rm Si}\rangle-\langle{\rm O}\rangle$, are easy to compute. On the other hand, the average instantaneous separations of neighbouring Si and O atoms, here labelled $\langle{\rm Si}-{\rm O}\rangle$, can be obtained by Fourier transformation of $S(\mathbf{Q})$. Our work using powder diffraction methods, obtaining the average positions by Rietveld refinement and the mean separations by calculation of the pair distribution functions from the Fourier transform of the full diffraction pattern, has shown that there is a significant discrepancy between $\langle{\rm Si}\rangle-\langle{\rm O}\rangle$ and $\langle{\rm Si}-{\rm O}\rangle$, which becomes larger on heating. This is illustrated in Fig. 1.

For a crystal, $S(\mathbf{Q})$ contains both the Bragg scattering and the diffuse scattering, the latter of which may arise from static defects or thermal motions. For this reason, $S(\mathbf{Q})$ is called the 'total scattering function'. Experimental measurements are much easier using polycrystalline samples than single crystals. This does not simply follow the notion that powder diffraction is easier than single-crystal diffraction. In using total scattering measurements to provide information about interatomic distances, we have to face the problem of resolution (the same problem exists in standard structure solution, but it is not often found to be necessary to confront it in this context!). The resolution in the Fourier transform of $S(Q)$ (assuming now the use of polycrystalline samples in which measurements are

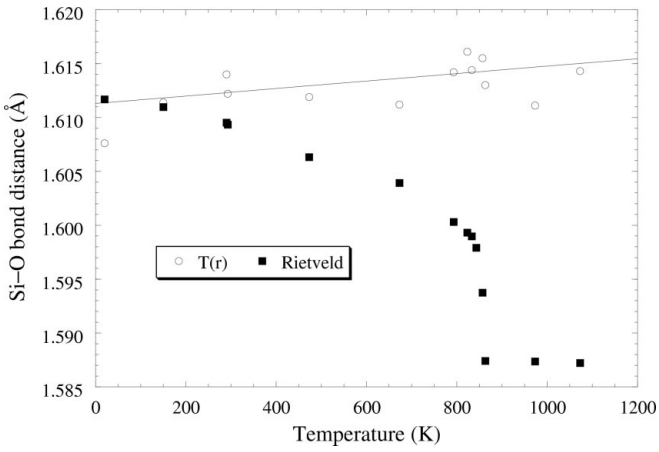

Figure 1
Comparison of the mean Si—O distance, ⟨Si—O⟩, in quartz, obtained from the $T(r)$ pair distribution function, and the distance between the mean positions of the Si and O distances, ⟨Si⟩—⟨O⟩, obtained from Rietveld refinement (Tucker *et al.*, 2000; Tucker, Keen & Dove, 2001). The important point is that the two distances quickly diverge on heating from 0 K, with ⟨Si—O⟩ showing a small increase on heating as a result of normal thermal expansion of the bond, whereas ⟨Si⟩—⟨O⟩ decreases on heating in a manner that appears to follow closely the distortion of the long-range structure caused by the phase transition.

performed as an average over all orientations of **Q**) is given by $2\pi/Q_{\max}$, where $Q_{\max}$ is the largest value of Q in the data. For a resolution of around 0.15 Å, which is around 10% of the closest interatomic separation, it is necessary to extend the data to a value of $Q_{\max}$ of slightly over 40 Å^{-1}. By comparison, the maximum possible value of Q using a standard Cu $K\alpha$ X-ray source is just over 8 Å. The increase in the range of Q by a factor of 5 would give an increase in the volume of reciprocal space by a factor of 125, and this massive increase in data for single-crystal diffraction, spread over the whole volume of reciprocal space rather than limited to the Bragg vectors, would be very difficult to handle in terms of collection, storage and analysis. As a result, there is much interest in using powder methods for collection of good $S(Q)$ data.

In this paper, we address some of the issues associated with the analysis of $S(Q)$ data from polycrystalline materials and the use of RMC methods for the study of disordered crystals. In many ways, the approach is very similar to that used in the study of liquids and amorphous materials, but for crystalline materials we can treat the Bragg scattering component as a separate set of data. The full $S(Q)$ data contain information about the distribution of interatomic separations and the Bragg diffraction data contain information about the single-particle distribution functions. The merit in combining both sets of data in the same analysis is that the final result is constrained with regard to both types of distribution function. This is a particular advantage that is clearly not available in the study of liquids and amorphous materials. We will present an approach to combine both sets of data within the framework of the RMC method. We will discuss one particular strategy and how the two sets of data together are able to lead to more reliable results from the RMC method.

Our approach is not the only one that has been applied to the study of crystalline materials by the RMC method. Mellergård & McGreevy (1999, 2000) recently presented an alternative approach, which we will discuss at the end of this paper (§6).

1.2. Common problems associated with the RMC method

The RMC method has not been accepted without some degree of controversy and there are two 'popular' criticisms of it. The first is the lack of a unique solution, which effectively means that there may be many configurations that give a good agreement with the experimental data. Some would argue that this 'problem' arises because often there are more variables in the configuration than data points in the measurements. There are two possible aspects to this issue. The first is that it is inevitable (and actually desirable) that many different configurations will match the experimental data. The configurations will contain only a few thousand atoms, whereas a sample in an experiment will contain of the order of 10^{24} atoms. The configuration can only ever reproduce a small subset of the atomic configurations that occur in a real sample. However, it would be hoped that the configurations produced by the RMC sample would give correlation functions that are in close agreement with those of the real sample. The $S(Q)$ data give pair correlation functions, but there is an infinite hierarchy of higher-order correlation functions (for example, the next level up would involve clusters of three atoms, such as the Si—O—Si cluster in a silica sample) that are not directly contained within the experimental data. If, in some untestable way, the RMC method could reasonably reproduce the complete hierarchy of correlation functions of the real sample, there is no problem with uniqueness. However, there is no guarantee that the form of the pair correlation functions can constrain any of the higher-order correlation functions appropriately, and if the RMC method were to generate configurations with the same pair correlation functions but quite different higher-order correlation functions, there is a true uniqueness problem that has to be faced.

The second criticism of the RMC method is that, in being based on methods in statistical thermodynamics, it is subject to rules such as the maximization of entropy. In effect, the RMC method will produce configurations with the largest amount of disorder possible, while remaining consistent with the pair correlation functions given by the experimental data. This problem is related to the uniqueness problem outlined above, *i.e.* there is no guarantee that the most disordered configurations that satisfy the constraints of the experimental pair distribution functions will be consistent with the true structure.

Because we have no experimental method to determine the higher-order correlation functions in a crystal directly, it cannot be possible to determine whether either of the aforementioned problems (uniqueness or maximum entropy) can be solved. However, it is possible to limit the scope of these problems by appropriate use of constraints at the lower end of the hierarchy of correlation functions; in this paper we outline some such approaches.

1.3. Outline of the paper

The main part of the paper has the following sequence. In the next section (§2) we describe our implementation of the RMC method for the study of crystalline materials. We follow the earlier idea of Keen (1997) of using bond constraints and we introduce a method of incorporating the intensities of Bragg peaks directly. We will discuss how the data can be treated in order to be able to incorporate these constraints and intensities together. Two examples, taken from recent studies on quartz and cristobalite, will be presented, including details of the experimental methods and some specific details of the corresponding RMC simulations (§3). This is followed by analysis of the roles of the different components of the data on the behaviour of the RMC simulation (§4). Finally, we present some results for quartz and cristobalite, focusing on both real-space configurations and the reciprocal-space analysis of diffuse scattering (§5). The paper is concluded with a brief discussion of an alternative approach to the application of the RMC method to crystalline materials (§6).

2. Developments of the RMC method for the study of crystalline materials

2.1. Overview of the basic equations

The basic equations for scattering from an isotropic material (such as a liquid, but also applying to a polycrystalline material) are (Keen, 2001):

$$S(Q) = \frac{1}{N}\frac{\mathrm{d}\sigma}{\mathrm{d}\Omega} = F(Q) + \sum_{i=1}^{n} c_i \overline{b_i^2}, \tag{3}$$

$$F(Q) = \rho_0 \int_0^\infty 4\pi r^2 G(r) \frac{\sin Qr}{Qr}\,\mathrm{d}r, \tag{4}$$

$$G(r) = \sum_{i,j=1}^{n} c_i c_j \bar{b}_i \bar{b}_j [g_{ij}(r) - 1], \tag{5}$$

$$T(r) = 4\pi r \rho_0 \Big[G(r) + \Big(\sum_{i=1}^{n} c_i \bar{b}_i \Big)^2 \Big]. \tag{6}$$

Equation (3) gives the intensity of the scattered beam. $F(Q)$ is the contribution from pairs of distinct atoms. $g_{ij}(r)$ is the pair distribution function, defined such that $g(r = 0) = 0$ and $g(r \rightarrow \infty) \rightarrow 1$. $G(r)$ combines the $g_{ij}(r)$ from different pairs of atoms, with c_i representing the amount of each atom. The final function, $T(r)$, has the functional form that is most closely related to the Fourier transform of $F(Q)$.

Finally, the intensity of a Bragg peak at $Q = |\mathbf{Q}_{hkl}|$ is given by

$$I_{\mathrm{Bragg}}(hkl) = m_{hkl} \Big| \sum_j b_j \exp(i\,\mathbf{Q}_{hkl} \cdot \mathbf{r}_j) \Big|^2, \tag{7}$$

where m_{hkl} is the multiplicity of the hkl reflection.

2.2. Basics of reverse Monte Carlo modelling

The RMC approach has been described in a number of articles (McGreevy & Pusztai, 1988; McGreevy, 1995; Keen, 1997, 1998). In the general approach, a starting configuration of atoms is produced with periodic boundaries, using either a random arrangement of atoms or the crystal structure. This starting configuration must have the correct density and contain the correct ratio of atoms, *i.e.* 1:2 for SiO_2. The RMC simulation then proceeds by moving an atom selected at random by an amount (within a set limit) also selected at random. Standard Monte Carlo procedures are used to test whether to accept or reject the move, through calculation of a change in an appropriate 'energy' function. In the general approach, the energy function can be associated with either or both of the following residuals:

$$\chi^2_{F(Q)} = \sum_i [F_{\mathrm{calc}}(Q_i) - F_{\mathrm{exp}}(Q_i)]^2 / \sigma^2_{F(Q_i)} \tag{8}$$

and/or

$$\chi^2_{T(r)} = \sum_i [T_{\mathrm{calc}}(r_i) - T_{\mathrm{exp}}(r_i)]^2 / \sigma^2_{T(r_i)}. \tag{9}$$

In both equations, σ is a weighting variable (often held constant for neutron scattering data), which may be taken to be the error of the particular point, or else may be set 'by hand'. Instead of using $F(Q)$ or $T(r)$ in the energy functions, it would be possible to use another of the real- or reciprocal-space functions associated with total scattering. Clearly it is necessary to calculate the functions $F_{\mathrm{calc}}(Q)$ and $T_{\mathrm{calc}}(r)$ after each step in order to make comparisons with the experimental quantities.

In using either of these approaches, any move that reduces χ^2 is accepted, and any move that increases χ^2 by an amount $\Delta\chi^2$ is accepted only with probability $\exp(-\Delta\chi^2/2)$. From the equations, it is clear that increasing the set of values of σ will enable more moves to be accepted. Once a move has been accepted or rejected, another move is proposed at random, and the process repeated. This sequence continues until it is clear that the energy function is oscillating about a stable low value.

In using $\chi^2_{F(Q)}$ in the RMC method, it has to be recognized that the finite size of the sample imposes some restrictions. The $T(r)$ function can be calculated only to a maximum value of r that is given by the smallest dimension of the RMC sample. Thus Fourier transformation of the $T(r)$ function over a restricted range of r will lead to significant truncation ripples and broadening in the computed $F(Q)$. To facilitate comparison of the experimental and calculated $F(Q)$ functions in the light of this problem, the experimental $F(Q)$ data are convoluted with the Fourier transform of the sample box function (see, for example, data in Fig. 2):

$$F^{\mathrm{conv}}_{\mathrm{exp}}(Q) = \frac{1}{\pi} \int_{-\infty}^{+\infty} F_{\mathrm{exp}}(Q') \frac{\sin[(Q - Q')L/2]}{Q - Q'}\,\mathrm{d}Q'. \tag{10}$$

The basic approach of the RMC simulation suffers particularly from the entropy problem outlined earlier. There may be many unrealistic configurations that will nevertheless give a reasonable reproduction of the experimental data overall, and discrepancies that are associated with very unreasonable local configurations of atoms may not contribute substantially to the energy function. As a result, it is useful to incorporate

some constraints. One of the simplest is to define a distance of closest approach for atoms, which can be enforced in the RMC simulation. This can be defined from known atomic or ionic radii, or taken from the experimental $T(r)$ function. Recently, Keen (1997, 1998) applied bond constraints to the RMC method. For silica, these consisted of constraints to ensure that the Si—O bond distances were not able to drift away from the known distances and constraints to ensure that the O—Si—O angles did not drift away from the ideal tetrahedral angle. These constraints are enforced by using the following energy function:

$$\chi^2_{\rm poly} = \sum_{\rm Si-O} |r_{\rm Si-O} - R_{\rm Si-O}|^2/\sigma^2_{\rm Si-O} + \sum_{\rm O-Si-O} |\theta_{\rm O-Si-O} - \Theta_{\rm O-Si-O}|^2/\sigma^2_{\rm O-Si-O}, \quad (11)$$

where $R_{\rm Si-O}$ is the expected mean Si—O distance and $\Theta_{\rm O-Si-O}$ is the ideal tetrahedral angle, 109.47°. By taking the value of $R_{\rm Si-O}$ from the first peak in the $T(r)$ data, the constraint is made to be data-based. Furthermore, if all weightings in the other χ^2 functions are given by the experimental errors, the value of $\sigma_{\rm O-Si-O}$ could reflect the width of the peak in $T(r)$.

The point of these constraints is to ensure that deformations of the SiO_4 tetrahedra in the final configuration are reduced to a minimum. This enabled the development of better RMC models for silica glass, starting from a random configuration of atoms. However, when the constraints are applied to crystalline materials with initial configurations obtained from the known crystal structure, the role of these constraints is to ensure that the SiO_4 tetrahedra are not unreasonably deformed by the RMC procedure. In short, they hold the tetrahedra together. One of us (Keen, 1997, 1998) has pointed out that when these constraints are applied to a structure formed from an initial crystal structure, the RMC procedure acts to 'refine' the average structure in the configuration, in contrast to the normal use of the RMC method, which produces models *via* a wider sampling of configuration space.

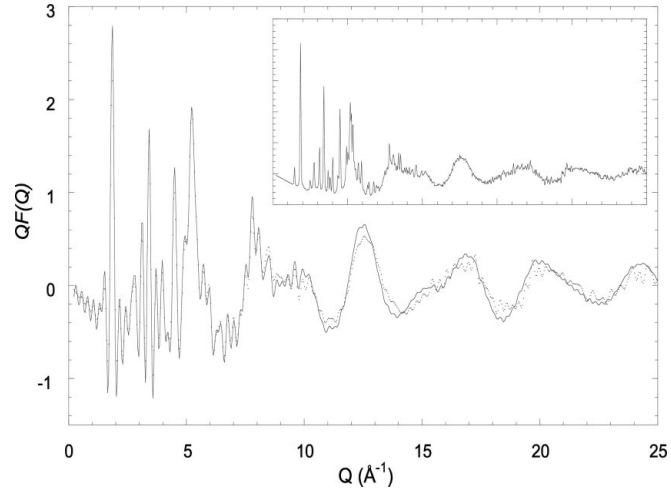

Figure 2
Measurements of $QF(Q)$ for β-quartz at 1073 K, convoluted with the Fourier transform of the sample shape function (points), along with the calculated function from the RMC refinement using all the data and constraints (curve). The inset shows the unconvoluted data.

2.3. Extension of the RMC method for crystalline materials

The RMC methods outlined above can be applied directly to crystalline materials, as we have described in earlier publications. However, we now have to face new aspects of the entropy issue. In a topologically disordered material, the entropy issue is concerned with generating structural disorder in terms of inappropriate local atomic coordinations. This does not present any problem for crystalline materials when the bond distance and bond angle constraints are used. However, although the local structures may be consistent with the $T(r)$ and $F(Q)$ data, it is still possible for the long-range structure to be different from the real structure. For example, the mean-square displacements of atoms from their average positions may not be properly modelled within the RMC procedure. Of course, the information on long-range order is contained within the Bragg peaks that are found in the $F(Q)$ data, but not in a useful form, because of the aforementioned problem with the effects of truncation on the Fourier transform of the calculated $T(r)$. This means that the resolution in the Fourier transform of $T(r)$ is broadened by roughly $2\pi/r_{\rm max}$ and the crystalline diffraction pattern resembles more that of an amorphous diffraction pattern (and we note that the diffraction from amorphous silica looks like that of crystalline β-cristobalite with a broadening of the Bragg peaks). The scattering associated with the Bragg peak will then be mixed with the diffuse scattering with similar Q. Specifically, it would be useful to separate the contribution from the elastic Bragg intensity,

$$I_{\rm Bragg}(Q) = \Big| \sum_j \bar{b}_j \langle \exp(i\,\mathbf{Q}\cdot\mathbf{r}_j)\rangle \Big|^2, \quad (12)$$

from that of the total scattering (Bragg plus inelastic),

$$I_{\rm total}(Q) = \Big\langle \Big| \sum_j \bar{b}_j \exp(i\,\mathbf{Q}\cdot\mathbf{r}_j)\Big|^2 \Big\rangle. \quad (13)$$

Our approach is to define a new energy function,

$$\chi^2_{\rm Bragg} = \sum_{hkl} |\alpha\, I^{\rm exp}_{\rm Bragg}(hkl) - I^{\rm calc}_{\rm Bragg}(hkl)|^2/\alpha^2\,\sigma(hkl)^2, \quad (14)$$

where $I^{\rm exp}_{\rm Bragg}(hkl)$ is the intensity of the hkl Bragg peak extracted using the Pawley (1981) method, and $I^{\rm calc}_{\rm Bragg}(hkl)$ is the intensity calculated using equation (7). $\sigma(hkl)$ is the estimated error of the extracted Bragg intensity. α is a scale factor. In principle, the value of α can be obtained from the normalization of the data, but if not, it can be treated as an adjustable parameter in the RMC procedure. Specifically, if the value of α is chosen to minimize $\chi^2_{\rm Bragg}$, it can be shown that it is given by

$$\alpha = \frac{\sum_{hkl} I^{\rm calc}_{\rm Bragg}(hkl)\, I^{\rm exp}_{\rm Bragg}(hkl)/\sigma(hkl)^2}{\sum_{hkl} I^{\rm calc}_{\rm Bragg}(hkl)^2/\sigma(hkl)^2}. \quad (15)$$

We can now obtain an overall χ^2 by summing over all the individual values:

$$\chi^2 = a_{F(Q)}\,\chi^2_{F(Q)} + a_{T(r)}\,\chi^2_{T(r)} + a_{\rm poly}\,\chi^2_{\rm poly} + a_{\rm Bragg}\,\chi^2_{\rm Bragg}, \quad (16)$$

where the coefficients $a_{F(Q)}$, *etc*., can be treated as switches that allow the particular set of data or constraints to be included or excluded. In this paper, we will explore the effects of including or excluding the different components of χ^2.

2.4. Overlap of information

It can be remarked that the different χ^2 functions in equation (16) have a considerable amount of overlap of the same information. For example, since $T(r)$ is obtained from $F(Q)$, there can hardly be any difference in the information content of the two functions. However, what is different is the weightings that both functions give to different aspects of the structure. Our use of $T(r)$ places special weight on the short-range structure, whereas $F(Q)$ is weighted across all length scales. Similarly, the information about the Bragg peaks is contained in $F(Q)$, but the effect of separating out $\chi^2_{\rm Bragg}$ is to unmix the information about the long-range order from the information about the short-range order. Moreover, the polyhedral constraints used in $\chi^2_{\rm poly}$ are generated by the $T(r)$ data, but by separating out the constraint terms, higher weight is added to the low-r part of $T(r)$ and the particular interpretation of this information [namely that the Si—O bond length and integral of the peak in $T(r)$ imply tetrahedral coordination of Si]. As well as direct information overlap, the different sets of data can provide constraints that impinge on other data sets. For example, in a perfectly ordered structure, the high degree of order seen in $T(r)$ at medium to long distances is likely to be modelled only by moving the atoms in a way that also gives agreement with $\chi^2_{\rm Bragg}$. Thus inclusion of $\chi^2_{\rm Bragg}$ will not provide a completely new data-based constraint on the refinement, but it will act in concert with the $T(r)$ data. On the other hand, in disordered materials, it is less likely that the individual terms in equation (16) will have such a high correlation with the other terms, and it is in these cases that the wide range of terms in equation (16) has particular value.

3. Details of experimental methods and RMC refinements

3.1. Experimental details

Total-scattering experiments were performed using both cristobalite and quartz as the samples, using the (now decommissioned) LAD diffractometer at the ISIS pulsed-neutron source (Howells & Hannon, 1999). Full details of the measurements are given elsewhere (Tucker *et al.*, 2000; Tucker, Keen & Dove, 2001). These include details of the standard procedures (Wright, 1993, 1997; Howe *et al.*, 1989) followed to correct the data for background scattering and to normalize the data to give an absolute measurement of $F(Q)$ for values of Q between 0.5 and 50 Å^{-1}. Data were collected at five temperatures for cristobalite (473–950 K) and at 13 temperatures for quartz (20–1073 K).

The $F(Q)$ data were converted to $T(r)$ using an inverse Monte Carlo method (Pusztai & McGreevy, 1997). This has the main advantage of reducing the termination ripples that arise from a standard Fourier transform. Fig. 2 shows $QF(Q)$ data for β-quartz at 1073 K, convoluted with the Fourier transform of the sample shape function [according to equation (10)] and fitted using the RMC refinement (as described earlier, with specific details given below). In Fig. 3, the corresponding transform to $T(r)$ is presented and compared with the function calculated by the RMC refinement.

In addition to converting the data to $F(Q)$, we also converted the data into a form suitable for Rietveld analysis and for extraction of the intensities of the Bragg peaks. Both procedures were performed using the *CCSL* code developed at ISIS (Brown & Matthewman, 1987; David *et al.*, 1992). Values of $I_{\rm Bragg}(hkl)$ were obtained from the powder diffraction data using the Pawley (1981) method, which also gives an associated error, up to a maximum Q of 12.5 Å^{-1}. In cases where there is overlap of a few peaks, the Pawley method will give the intensity of a group of reflections. However, at higher values of Q, there may be considerable overlap of reflections with no clear structure in the diffraction pattern; then it is not possible to extract Bragg intensities. In this approach, the Lorentz factor is removed as part of the same process.

Rietveld analysis was used to obtain accurate lattice parameters, needed to define the size and shape of the atomic configuration used in the RMC modelling. When comparing the average atomic positions from the RMC refinements, it is probably most sensible to compare them with the results of the Rietveld refinement from the same basic set of data.

3.2. Reverse Monte Carlo refinements

The starting point for each RMC refinement was a sample containing 10 × 10 × 10 unit cells with orthogonal axes. For quartz, this meant an orthorhombic supercell of the trigonal or hexagonal structure, with 18000 atoms in the sample; for cubic β-cristobalite, the sample contained 24000 atoms, while for tetragonal α-cristobalite, the sample contained 12000 atoms. In each case, the lattice parameters and starting positions for the atoms were those given by the preliminary Rietveld

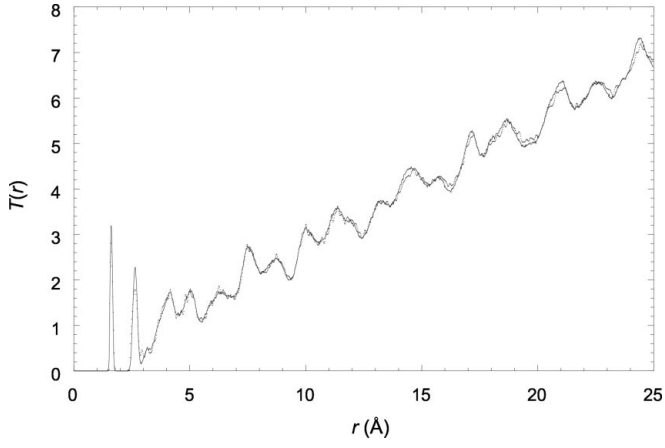

Figure 3
$T(r)$ for β-quartz at 1073 K (points), with the fitted function from the RMC refinement using all the data and constraints (curve).

Table 1
Definitions of the χ^2 terms used in test RMC refinements.

Refinement name	χ^2 terms used
Raw	Initial configuration, not refined
Polyhedra	$\chi^2_{\rm poly}$
Bragg	$\chi^2_{\rm poly} + \chi^2_{\rm Bragg}$
$F(Q)$	$\chi^2_{\rm poly} + \chi^2_{F(Q)}$
$F(Q)$ + Bragg	$\chi^2_{\rm poly} + \chi^2_{F(Q)} + \chi^2_{\rm Bragg}$
$T(r)$	$\chi^2_{\rm poly} + \chi^2_{T(r)}$
$T(r)$ + Bragg	$\chi^2_{\rm poly} + \chi^2_{T(r)} + \chi^2_{\rm Bragg}$
$T(r)$ + $F(Q)$	$\chi^2_{\rm poly} + \chi^2_{T(r)} + \chi^2_{F(Q)}$
No polyhedral constraints	$\chi^2_{T(r)} + \chi^2_{F(Q)} + \chi^2_{\rm Bragg}$

refinements. The RMC refinement using the full χ^2 function of equation (16) was run for 80 h on a Silicon Graphics R5000 processor, and the test refinements excluding different contributions to equation (16) were each run for 40 h. The refinement for 80 h generated ~1.5 million atom moves, with an acceptance rate of around 1/3. The values of σ in the equations for χ^2 were held fixed throughout the refinements. In principle, the values could be systematically reduced during the refinement procedure, as in standard simulated-annealing methods, but in practice a good set of values could be preselected from earlier experience, and it was found not to be necessary to force them to vary.

4. Tests of the different contributions to equation (16)

4.1. Quality of the refinements

In order to investigate the effects of the different terms in the expression of χ^2 by equation (16), a number of test RMC refinements were carried out in which selected contributions were excluded. The data used for these tests were from quartz at 20 K and 1073 K; these two data sets were chosen since they are the two end members of the series of measurements spanning the α–β phase transition, and as such represent materials with low and high thermal disorder. Initially, both sets of data were refined using the total χ^2 of equation (16); these results were then used as a standard against which to measure the quality of subsequent refinements. Table 1 presents the different refinements that were performed. After 40 h of fitting, all the individual χ^2 terms in equation (16) were calculated for each configuration and scaled according to the results obtained with all contributions included. The results are plotted in Fig. 4 in the form of a bar chart. The name of the refinement is given on the vertical axis and $\chi^2/\chi^2_0 - 1$ is plotted on the horizontal axis, where χ^2_0 is obtained from the standard refinements with all contributions included. With the data plotted in this way, when the magnitude of the bars is negative, the fit with that model is better, and *vice versa* when the bar magnitude is positive. The oscillation when equilibrium has been reached would give a bar of magnitude 0.05 on the scale of this bar chart.

If we compare the refinements labelled 'Raw' and 'Polyhedra', the former being the initial configuration and the latter being a refinement using the polyhedra constraints without the diffraction data directly [although we noted above that the polyhedra constraints are generated by the $T(r)$ data], we see from Fig. 4 that the constraints on the size and shape of the SiO_4 tetrahedra have a large effect on the final fit. Effectively, we have allowed the tetrahedra to move as nearly rigid units in a random way, which to some extent mimics thermal disorder. The effects are particularly large for the data at 1073 K, where it is known that the values of $\langle$Si$\rangle$—$\langle$O$\rangle$ obtained from the Rietveld refinements are significantly lower than the values of $\langle$Si—O$\rangle$ obtained from the $T(r)$ data (Tucker *et al.*, 2000). The effects are not negligible for the 20 K data either, although they are considerably smaller, because it is known that the α-quartz structure still contains some degree of framework flexibility (Hammonds *et al.*, 1996), which allows motion of the tetrahedra in the refinement.

By way of contrast, the refinement labelled 'No polyhedra constraints', which takes account of all direct diffraction data but without the contribution $\chi^2_{\rm poly}$, gives low values for the data χ^2 but high values of $\chi^2_{\rm poly}$, as seen in Fig. 4. It appears that the polyhedra constraints are needed to prevent the polyhedra from distorting. It should be noted that some degree of polyhedra distortion is generated in the 20 K refinement, even though the agreement with the $T(r)$ data appears to be good. For the remaining tests, we always include $\chi^2_{\rm poly}$.

The addition of only the $\chi^2_{\rm Bragg}$ term, labelled 'Bragg' in Table 1 and in Fig. 4, improves the fit to the Bragg data but appears to have little effect on the other terms in the overall χ^2 expression. In contrast, inclusion of the $F(Q)$ data without the Bragg intensity data in the RMC refinement, namely the case labelled '$F(Q)$' in Table 1 and Fig. 4, has an effect on both $\chi^2_{F(Q)}$ and $\chi^2_{\rm Bragg}$. Inclusion of both $\chi^2_{F(Q)}$ and $\chi^2_{\rm Bragg}$ in the fit, the case labelled '$F(Q)$ + Bragg', gives an even lower value of $\chi^2_{\rm Bragg}$. The point is that some information about the long-range structure as seen in the intensities of the Bragg peaks is included in $F(Q)$, as expected, but by separating the Bragg peaks from the total diffraction data, the refinement is able to match the long-range order better.

An analogous picture is seen with the $T(r)$ data alone [labelled '$T(r)$'] and with a combination of the $T(r)$ and Bragg intensity data [labelled '$T(r)$ + Bragg']. The $T(r)$ data alone lead to a reduction of $\chi^2_{\rm Bragg}$. There is a greater reduction when the Bragg intensity data are included. By comparing the two sets of refinements with either the $F(Q)$ or the $T(r)$ data, it can be seen than the corresponding values of χ^2 are different in each case. This reflects the different weightings exerted by the two functions, as discussed above.

The final result concerns the effect of including or not including the Bragg intensities when both the $F(Q)$ and the $T(r)$ data are used in the RMC refinement. It can be seen that there is only a marginal improvement when including the Bragg intensity data (more so for the 1073 K data). The point of including the Bragg intensity data is not to provide an improved RMC refinement *per se*, but to instil more confidence in the realism of the configurations generated by the refinement. That the inclusion of the Bragg intensity data has only a small effect shows that the information about the long-range order is obtained from the combined use of the $T(r)$ and

$F(Q)$ data, but the cases when we did not use the combined data did show that it is possible for the Bragg intensity to have a significant effect on the RMC refinement. In the present example, the inclusion of the Bragg intensities has increased our confidence in the outcome of the RMC refinement, but we anticipate that there may be cases where it has a real effect on the final configurations. The issue of confidence is important in the light of the earlier discussion about the possibility that the RMC method can generate too much disorder.

To summarize the results of these tests, the main effects on the RMC refinements arise from the bond constraints. When also using either the $F(Q)$ or the $T(r)$ data with the constraints, inclusion of the Bragg intensity data improves agreement with the data. When using both the $F(Q)$ and the $T(r)$ data with the constraints, inclusion of the Bragg intensity data has less effect, but improves our confidence in the final model. Two things should be noted about this point. First, we should reiterate the need for models of structural disorder to be formed within the scheme of the average structure; models which do not reproduce the Bragg intensities should be questioned. Secondly, part of the reason that the $F(Q)$ and $T(r)$ models described here produce good agreement without recourse to the Bragg constraint is that the data are of high quality. With more limited data (*e.g.* a smaller Q range), the Bragg constraints may be more important. The tests show a correlation with the temperature at which the data were collected. The 20 K data correspond to an ordered structure, while the 1073 K data correspond to a disordered structure. In the ordered structure, the local structure produced by the $T(r)$ data is able to constrain the long-range order, which is why the $T(r)$ data have a significant effect on the agreement with all data sets at low temperature, but not at high temperature, as seen in Fig. 4.

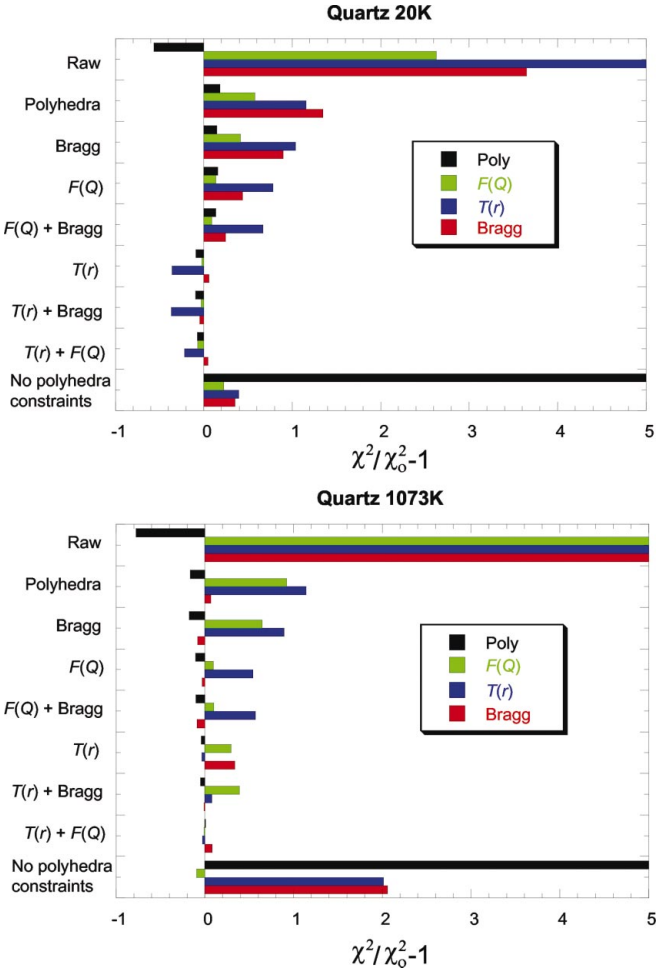

Figure 4
Results of the tests based on different combinations of data using the RMC refinements, as defined in Table 1.

4.2. Speed of convergence

During the study of cristobalite, it was noticed that the inclusion of the Bragg intensities had a significant effect on the speed at which the RMC refinement converged to an equilibrium value of χ^2. Whereas it might be expected that including an additional energy term in the refinement might increase the computational time per step, it was found that the total time for the simulation to reach equilibrium was reduced. Fig. 5 shows the value of χ^2 plotted against CPU time for the simulations that included or excluded the Bragg peak intensities. This shows how the Bragg peak intensities increase the speed of convergence. The inset in Fig. 5 gives the number of moves generated during the refinements. The rate at which moves are performed is slightly less where the Bragg intensities have to be calculated, since it takes longer to calculate the extra parameter for each move. This shows that equilibrium is achieved in fewer moves as well as in less time in the case where the Bragg intensities are included explicitly. The interpretation is that the Bragg intensities exert additional constraints on the model, so that moves that cause the average structure to deviate are not accepted. This ensures that the path to a final fit is smoother and thus quicker. Wicks *et al.* (1997) noted a similar effect when using appropriate coordination constraints for a glass.

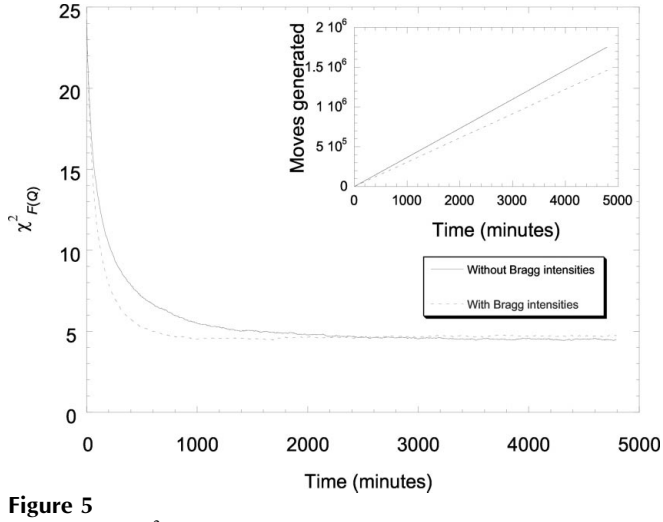

Figure 5
Variations of χ^2 without Bragg constraints (solid line) and with Bragg constraints (dashed line) with CPU time used. The inset graph shows the total number of moves generated with time.

5. Sample results using the RMC refinement method

5.1. Quartz

The results of the RMC refinements on quartz are shown in Fig. 6 as cuts through the final three-dimensional configurations. The insets give the average structures of α- and β-quartz as obtained from the RMC refinements. These are consistent with the results of the Rietveld refinements and with the average structures. The α-quartz configuration produced at 20 K shows very little disorder. This, of course, is expected at such a low temperature. However, since the RMC method moves the atoms in the configuration randomly through hundreds of thousands of steps, it is not obvious, *a priori*, that the RMC refinement would retain the ordered structure. This example shows that the data and constraints include enough information to produce the universally accepted ordered structure. On the other hand, it might then be possible that the data and constraints could over-constrain the simulation, giving no room for disorder. That this is not the case is shown by the configuration obtained from the 1073 K data. Here the picture is of a structure that contains a high degree of local disorder, while remaining consistent with the higher-symmetry average structure of β-quartz. It is clear from the comparison of the RMC configuration with the average structure that the local disorder is achieved through rotations of the SiO_4 tetrahedra. More detailed analysis of the RMC refinements across the whole range of temperatures is discussed in detail elsewhere (Tucker *et al.*, 2000; Tucker, Keen & Dove, 2001).

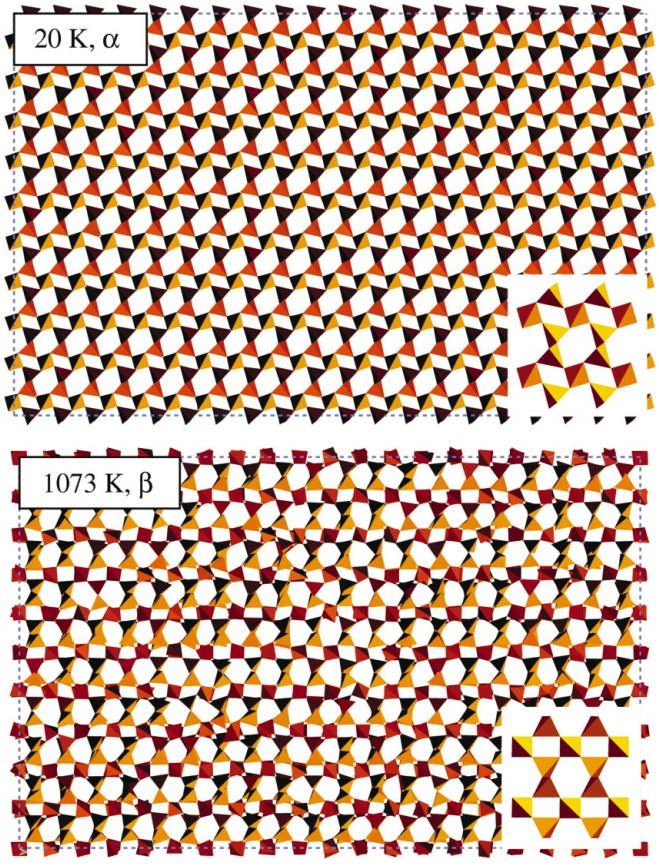

Figure 6
(100) layers of instantaneous RMC atomic configurations of quartz represented by SiO_4 tetrahedra for one temperature above T_c and two below. The inserts show the 'average' structures obtained from the same configurations. In this projection, the small parallelopiped gaps between tetrahedra become orthogonal in the β-phase, giving a clear representation of the symmetry change at T_c.

5.2. Cristobalite

The second system investigated with this new structure refinement method was cristobalite, the α and β phases of which were simulated. From the detailed analysis of Tucker, Squires *et al.* (2001), calculations of the three-dimensional diffuse scattering from the RMC configurations were selected, covering all temperatures. Sample results are shown in Fig. 7, where they are compared with the experimental data of Hua *et al.* (1988) and Welberry *et al.* (1989) for β-cristobalite. The agreement between the calculated and measured diffuse scattering of the β phase is very good, with the RMC refinement picking up the streaks of diffuse scattering with the correct intensity modulation.

Once again it might be thought that the random nature of the RMC approach produces diffuse scattering because of its natural ability to produce the most disordered structure that is consistent with the data and constraints. The fact that the Bragg intensities are now being fitted reduces the likelihood that this is the case. Furthermore, the pattern and intensity of the diffuse scattering calculated for the α-cristobalite config-

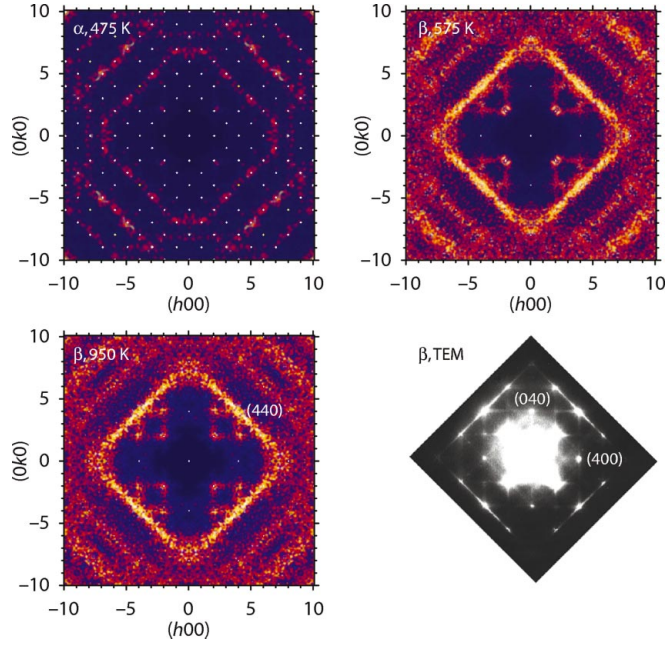

Figure 7
Maps of the three-dimensional diffuse scattering from cristobalite, showing the a^*–b^* plane in reciprocal space. The plot for α-cristobalite is indexed as β-cristobalite in order to highlight the common aspects. The single-pixel white spots are the Bragg peaks. The intensity scale of the diffuse scattering, as indicated by the shading (light for higher intensity, dark for lower intensity) is the same for all plots. The plot in the bottom right-hand corner represents experimental TEM measurements for β-cristobalite (Hua *et al.*, 1988; Welberry *et al.*, 1989).

uration is clearly different from that of the β-phase configuration (all plots in Fig. 7 are on the same scale). It is known from the RMC analysis (Tucker, Squires *et al.*, 2001) and other experiments that β-cristobalite is more disordered than the α phase, and the RMC refinements are able to respond to the data and constraints to produce the correct degree of order or disorder.

6. Discussion

The tests and results show that the RMC method can be applied successfully to crystalline solids. The new development in this paper is to take explicit account of the intensities of the Bragg peaks extracted from the diffraction pattern using the Pawley (1981) method. Our tests showed that if either $F(Q)$ or $T(r)$ are used as the primary data, the inclusion of the Bragg peaks plays a significant role in changing the degree of long-range order in the RMC configurations. For the examples described here, the inclusion of the intensities of the Bragg peaks has less effect when both $F(Q)$ and $T(r)$ data are used in the RMC method, but the inclusion of the Bragg peak data increases the confidence that the configurations do not suffer from increased disorder. This is backed up by the examples that cover a range of inherent structural disorder. Both examples are network structures, where the constraints play a large role. The Bragg peaks may play a more direct role in cases where such a three-dimensional network is not present.

As mentioned before, the application of the RMC method to crystalline materials has also been tackled by Mellergård & McGreevy (1999, 2000). These authors took a different approach. In their approach, called RMCPOW, the three-dimensional scattering is calculated (*cf.* the calculation of the total scattering shown for one reciprocal-lattice plane in Fig. 7) over a uniform grid in **Q**; then the three-dimensional diffuse scattering is reduced to the one-dimensional $F(Q)$. This approach differs from ours in that we separate out the intensities of the Bragg peaks explicitly, whereas in RMCPOW these are folded into the calculated $F(Q)$ data with no real loss of Q-space resolution. The data presented here extend to a high Q value. The application of RMCPOW over this entire Q range would be computationally prohibitive; therefore, in this instance, our method would be more efficient.

We are grateful for support from EPSRC.

References

Brown, P. J. & Matthewman, J. C. (1987). Rutherford Appleton Laboratory Report RAL-87-010.
David, W. I. F., Ibberson, R. M. & Matthewman, J. C. (1992). Rutherford Appleton Laboratory Report RAL-92-032.
Hammonds, K. D., Dove, M. T., Giddy, A. P., Heine, V. & Winkler, B. (1996). *Am. Miner.* **81**, 1057–1079.
Howe, M. A., McGreevy, R. L. & Howells, W. S. (1989). *J. Phys. Condensed Matter*, **1**, 3433–3451.
Howells, W. S. & Hannon, A. C. (1999). *J. Phys. Condensed Matter*, **11**, 9127–9138.
Hua, G. L., Welberry, T. R., Withers, R. L. & Thompson, J. G. (1988). *J. Appl. Cryst.* **21**, 458–465.
Keen, D. A. (1997). *Phase Transit.* **61**, 109–124.
Keen, D. A. (1998). *Local Structure from Diffraction*, edited by M. F. Thorpe & S. J. L. Billinge, pp. 101–109. New York: Plenum.
Keen, D. A. (2001). *J. Appl. Cryst.* **34**, 172–177.
McGreevy, R. L. (1995). *Nucl. Instrum. Methods A*, **354**, 1–16.
McGreevy, R. L. & Pusztai, L. (1988). *Mol. Simul.* **1**, 359–367.
Mellergård, A. & McGreevy, R. L. (1999). *Acta Cryst.* A**55**, 783–789.
Mellergård, A. & McGreevy, R. L. (2000). *Chem. Phys.* **261**, 267–274.
Pawley, G. S. (1981). *J. Appl. Cryst.* **14**, 357–361.
Pusztai, L. & McGreevy, R. L. (1997). *Physica B*, **234–236**, 357–358.
Tucker, M. G., Dove, M. T. & Keen, D. A. (2000). *J. Phys. Condensed Matter*, **12**, L723–L730.
Tucker, M. G., Keen, D. A. & Dove, M. T. (2001). *Miner. Mag.* **65**, 489–507.
Tucker, M. G., Squires, M. D., Dove, M. T. & Keen, D. A. (2001). *J. Phys. Condensed Matter*, **13**, 403–423.
Welberry, T. R., Hua, G. L. & Withers, R. L. (1989). *J. Appl. Cryst.* **22**, 87–95.
Wicks, J. D., McGreevy, R. L. & Borjesson, L. (1997). *Phase Transit.* **61**, 195–213.
Wright, A. C. (1993). *Experimental Techniques of Glass Science*, edited by C. J. Simmons & O. H. El-Bayoumi, pp. 205–314. *Ceramic Transactions*. Westerville: American Ceramic Society.
Wright, A. C. (1997). *Amorphous Insulators and Semiconductors*, edited by M. F. Thorpe & M. I. Mitkova, pp. 83–131. Dordrecht: Kluwer.